Optical Characterization of Infrared Emitting Rare-Earth-Doped Fluoride Nanocrystals and Their Transparent Nanocomposites

G. A. Kumar,[†] C. W. Chen,[†] J. Ballato,[‡] and R. E. Riman*,[†]

Department of Materials Science & Engineering, Rutgers—The State University of New Jersey, 607 Taylor Road, Piscataway 08854-8065, New Jersey, and Center for Optical Materials Science and Engineering Technologies (COMSET) and the School of Materials Science and Engineering, Clemson University, Clemson, South Carolina 29634

Received July 18, 2005. Revised Manuscript Received December 7, 2006

Nanocrystalline LaF_3:Nd and CaF_2:Er with rare-earth concentrations ranging from 0.5 to 16.7 mol % and dispersible particle sizes less than 100 nm were synthesized by solvothermal synthesis. Optical absorption, emission, and quantum efficiency were measured for the nanocrystals. Dopant levels of 0.5 mol % rare earth exhibited the best emission characteristics, with maximum quantum efficiencies of 95 and 51% for LaF_3:Nd and CaF_2:Er, respectively. The nanopowders were suspended in PFCB (6F variant) polymer-in-toluene solutions to make transparent suspensions that could be cast to make transparent nanocomposites. Scattering analysis indicates that the excellent transmission can be attributed to nanocrystals dispersed in the composite at length scales less than 100 nm.

Introduction

Nanomaterials captivate the materials world with the promise of exciting applications in science and technology. Unique physical, electronic, and chemical properties in the nanoregime presage the application of nanomaterials in the fabrication of optical, electronic, and biomedical devices. It is expected that optical nanomaterials will reduce the size and cost of many consumer and military devices by orders of magnitude. One reason is because nanomaterials can be blended into organic matrices where the resulting optical nanocomposite can assume the properties of the nanomaterials filler yet be processed with the low cost and ease of polymeric materials. In this paper, we will present work that focuses on luminescent optical nanocomposites based on rare-earth-doped nanopowders.

Luminescent materials based on rare-earth ions attract a great deal of attention nowadays because of their potential technological applications for displays, X-ray imaging, solid-state lasers, and optical amplifiers.[1−3] Among various rare earths, trivalent erbium and neodymium are of great interest because they emit in the third (1.5 μm) and second (1.3 μm) optical communication windows. Their luminescence arises from the parity forbidden intraconfigurational f → f transitions within their 4f shells. In this study, LaF_3 and CaF_2 were chosen as the hosts because of their low vibrational energies (280 cm^{-1} for CaF_2 and 350 cm^{-1} for LaF_3).[4,5] Resultantly, the quenching of the rare-earth-ion excited states will be minimal, yielding high quantum efficiency (bright emission). Er and Nd are important among the various rare earths because of their characteristic infrared emission properties at 1550 nm (Er^{3+}) and various emission lines for the 900−1800 nm (Nd^{3+}) range.

Research activity for nanocomposites has increased recently over the last 5 years. Ballato and Riman[6] reported and patented[7,8] the concept of transparent optical nanocomposites where all particles must be dispersed at length scales less than 100 nm. For intense optical emission, the importance of low phonon energy hosts were first reported and demonstrated for rare-earth-doped lanthanum chlorides[9,10] and lanthanum fluorides.[6] Since then, the synthesis and optical characterization of many rare-earth-doped nanoparticles have been reported.[11−23] The synthesis and optical

* Corresponding author. E-mail: riman@rci.rutgers.edu.
[†] Rutgers—The State University of New Jersey.
[‡] Clemson University.

(1) Blasse, G.; Grabmaier, B. C. *Luminescent Materials*; Springer Verlag: Berlin, 1994.
(2) Reisfeld, R.; Jorgensen, C. K. *Laser and Excited State of Rare Earths;* Springer Verlag: Berlin, 1977.
(3) Dejneka, M.; Samson, B. *MRS Bull.* **1999**, *8*, 39.
(4) Srivastava, P. J.; Singh, R. E. *J. Phys. C: Solid State Phys.* **1971**, *4*, L47.
(5) Reisfeld, R. Glass lasers and Solar Applications. In *Spectroscopy of Solid State Laser Type Materials;* Di Bartolo, B., Ed.; Plenum Press: New York, 1987; p 343.
(6) Ballato, J. Sol-Gel Synthesis of Rare-Earth-Doped Halide Optical Materials for Photonic Applications. Ph.D. Thesis, Rutgers University, New Brunswick, NJ, 1997.
(7) Riman, R. E.; Ballato, J. Rare Earth Doped Host Materials. U.S. Patent No. 6,699,406, March 2, 2004.
(8) Riman, R. E.; Ballato, J. Optically Transparent Nanocomposite Materials, U.S. Patent No. 7,094,361, August 22, 2006.
(9) Kumar, G. A.; Riman, R.; Snitzer, E.; Ballato, J. *J. Appl. Phys.* **2004**, *95*, 40.
(10) Ballato, J.; Riman, R. E.; Snitzer, E. *Opt. Lett.* **1997**, *22*, 691.
(11) Riwotzki, K.; Meyssami, H.; Kornowski, A.; Haase, M. *J. Phys. Chem. B* **2000**, *104*, 2824.
(12) Riwotzki, K.; Meyssami, H.; Schnablegger, H.; Kornowski, A.; Haase, M. *Angew. Chem., Int. Ed.* **2001**, *40*, 573.
(13) Lehmann, O.; Kompe, K.; Haase, M. *J. Am. Chem. Soc.* **2004**, *126*, 14942.
(14) Kompe, K.; Borchert, H.; Storz, J.; Lobo, A.; Adam, S.; Moller, T.; Haase, M. *Angew. Chem., Int. Ed.* **2003**, *42*, 5513.
(15) Heer, S.; Lehmann, O.; Haase, M.; Gudel, H. U. *Angew. Chem., Int. Ed.* **2003**, *42*, 3179.
(16) Lehmann, O.; Meyssamy, H.; Kompe, K.; Schnablegger, H.; Haase, M. *J. Phys. Chem. B* **2003**, *107*, 7449.
(17) Heer, S.; Kompe, K.; Gudel, H. U.; Haase, M. *Adv. Mater.* **2004**, *16*, 2102.

10.1021/cm051567n CCC: $37.00
Published on Web 02/28/2007

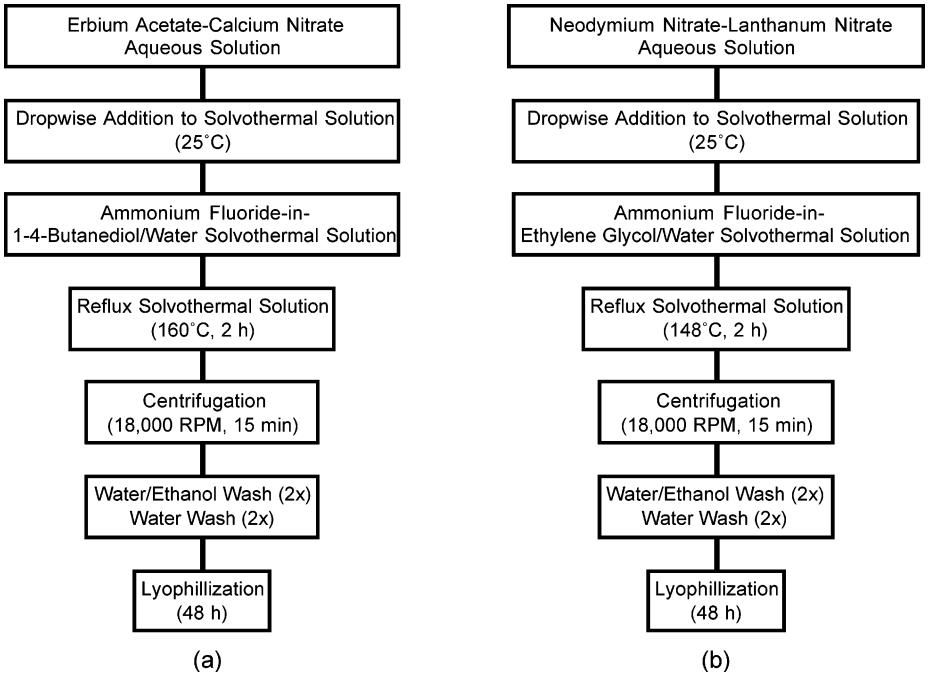

Figure 1. Flow chart for the solvothermal method of preparation of (a) CaF_2:Er and (b) LaF_3:Nd nanoparticles.

characterization of surface-coated rare-earth-doped LaF_3 nanoparticles with good dispersion in organic solvents was reported recently.[24,25] Capping agents such as ammonium di-*n*-octadecyl di-thiophosphate were used to control the particle growth and stabilize the particle against agglomeration. The stimulated emission and optical gain characteristics of neodymium-doped lanthanum fluoride (LaF_3:Nd) poly(methyl methacrylate) PMMA nanocomposite waveguides were reported by Dekker et al.[26] However, PMMA is not an appropriate polymeric matrix due to its strong absorptions in the 1600−1700 nm region, which contributes significant loss and noise to the optical spectrum. Recently we reported the fluorescence spectral and optical gain characteristics of CaF_2:Er/PFCB (perfluorocyclobutyl polymers, 6F variant) polymer−ceramic nanocomposites.[27] These materials are consistent with the requirement specified by refs 6−8, demonstrating the importance of using a polymer that is optically transparent in the region of the excitation and emission wavelengths for the rare earth of interest. In this paper, we report the optical properties of solvothermally derived CaF_2:Er and LaF_3:Nd nanocrystals and their nanocomposites in solution and the 6F variant PFCB (PFCB-6F) polymer.

(18) Riwotzki, K.; Haase, M. *J. Phys. Chem. B* **2001**, *105*, 12709.
(19) Hasse, M.; Riwotzki, K.; Meyssamy, H.; Kornowski, A. *J. Alloys Compd.* **2000**, *303*, 191.
(20) Meyssamy, H.; Riwotzki, K.; Kornowski, A.; Naused, S.; Hasse, M. *Adv. Mater.* **1999**, *11*, 840.
(21) Zhou, J.; Wu, Z.; Zhang, Z.; Liu, W.; Dang, H. *Wear* **2001**, *249*, 333.
(22) Yi, G.-S.; Chow, G.-M. *J. Mater. Chem.* **2005**, *15*, 4460.
(23) Stouwdam, J. W.; Raudesepp, M.; Van Veggel, F. C. J. M. *Langmuir* **2004**, *20*, 11763.
(24) Stouwdam, J. W.; Hebbink, G. A.; Huskens, J.; Van Veggel, F. C. J. M. *Chem. Mater.* **2003**, *15*, 4604.
(25) Stouwdam, J. W.; Van Veggel, F. C. J. M. *Nano Lett.* **2002**, *2*, 733.
(26) Dekker, R.; Klunder, D. J. W.; Borreman, A.; Diemeer, M. B. J.; Worhoff, K.; Driessen, A.; Stouwdam, J. W.; Van Veggel, F. C. J. M. *Appl. Phys. Lett.* **2004**, *85*, 6104.
(27) Kumar, G. A.; Chen, C. W.; Riman, R. E.; Chen, S.; Smith, D.; Ballato, J. *Appl. Phys. Lett.* **2005**, *86*, 241105

Experimental Section

Synthesis and Particle Characterization. Process flow charts are shown in Figure 1a,b to describe the nanoparticle synthesis procedure. CaF_2:Er nanocrystals were prepared solvothermally with Er^{3+} concentrations ranging from 0.5 to 16.7 mol %. At room temperature, a solution of $Er(OAc)_3$ (0.08 mmol, Aldrich, Milwaukee, WI) and $Ca(NO_3)_2$ (4 mmol, Aldrich, Milwaukee, WI) in 16 mL of water was added dropwise into stirred NH_4F (9 mmol, Acros Organics, Morris Plains, NJ) and 1,4-butanediol (99+%, Acros Organics) in water solution. The volume ratio of 1,4-butanediol/water was 4.3:1. Nd-doped LaF_3 samples with a Nd concentration of 0.5−10.7 mol % were prepared in ethylene glycol/water mixtures. At room temperature, a solution of $Nd(NO_3)_3$ (0.3 mmol, Aldrich, Milwaukee, WI) and $La(NO_3)_3$ (6 mmol, Aldrich, Milwaukee, WI) in 20 mL of water was added dropwise into stirred NH_4F (20 mmol, Acros Organics, Morris Plains, NJ) and ethylene glycol (reagent grade, Fisher Scientific, Pittsburgh, PA) in water solution. The volume ratio of ethylene glycol/water was 7:1. Both systems were stirred at the refluxing temperature, which corresponded to 148 °C for the ethylene glycol/water solution and 160 °C for the 1,4-butanediol/water solution. Refluxing was maintained for 2 h, and suspensions were subsequently cooled to room temperature. The precipitate was separated by centrifugation (Induction Drive Centrifuge, model J2-21M, Beckman Instruments, Palo Alto, CA) for 15 min at 18 000 rpm. The centrifuge cake was redispersed ultrasonically (FS-30, Fisher Scientific) and washed subsequently with 50 vol % of ethanol in water twice followed by a two-cycle deionized water wash (18.2 MΩ•cm, Millipore RiOs and Elix water purification system, Millipore Corporation, Burlington, MA). The product was lyophilized for 48 h (model FO-20-85 BMP Freezer Dryer, FTS Systems, Inc., Stone Ridge, NY). Portions of each powder were subsequently heat-treated at 800 °C in air at a rate of 50 °C/min (model BF51866A, Lindberg/Blue M, Asheville, NC) for 2 h.

Nanocomposites were prepared using solvent-based polymer processing methods. A PFCB polymer with a hexafluoropropyl derivative in the main chain (6F) was prepared by Tetramer

Technologies, LLC (Clemson, SC).[28] Toluene was used as the solvent for the preparation of the nanocomposites. Heat-treated powder was used for preparation of the polymer suspensions. A total of 0.168 g of PFCB-6F polymer was dissolved in 0.5 mL of toluene. A total of 0.0187 g of either Er-doped CaF_2 or Nd-doped LaF_3 was mixed with 0.5 mL of toluene and ultrasonicated (model FS-30, Fisher Scientific Co.) for 15 min. The suspensions were mixed with the above PFCB-6F polymer solution by ultrasonic mixing for 15 min.

X-ray diffraction (XRD) measurements were carried out with a Kristalloflex D-500 powder diffractometer (Bruker Axis, Inc., Madison, WI) using Ni-filtered Cu Kα radiation. The samples were scanned in the 2θ range of 10−80°, at a step size of 0.05°/step. Crystallographic identification of the heat-treated powders was accomplished by comparing the experimental XRD patterns to standards ((PDF no. 75-0363 for CaF_2, PDF no. 33-0704 for LaF_2, and PDF no. 32-0483 for LaF_3) compiled by the International Center for Diffraction Data (ICDD, Newtown Square, PA). The particle size and morphology were determined on a transmission electron microscope (TEM model EM-002B, International Scientific Instruments, Pleasanton, CA) operated at an accelerating voltage of 200 kV. The specimens were prepared by slow evaporation of a droplet of the nanoparticle-in-ethanol suspension onto a copper grid with an amorphous carbon film (Ernest Fullam, Inc., Latham, NY).

Optical Characterization. The optical absorption spectrum was recorded using a Perkin-Elmer spectrophotometer (Perkin-Elmer Lambda 9, Wellesley, MA) by dispersing the powder in ethanol. Luminescence spectra were recorded by exciting the powder sample with the 980 nm band using a semiconductor laser (model 980, Coherent, Inc., Santa Clara, CA) for CaF_2:Er and 800 nm from a titanium−sapphire ring laser (model 899-01, Coherent Inc., Santa Clara, CA) for LaF_3:Nd. The infrared emission was collected, focused, and dispersed using a 0.55 m double monochromator (Triax 550, Jobin Yvon, Edison, NJ). The signals were detected with a thermoelectrically cooled InGaAs detector (EO systems, Phoenixville, PA). A lock-in amplifier (Stanford Research System, model SR 850 DSP, Stanford, CA) amplified the output signal of the InGaAs detector. The spectrometer and the detection system were interfaced by a data acquisition system controlled with Spectramax commercial software (GRAMS 32, Galactic Corp., Salem, NH). Luminescence decay times were measured by modulating the laser with a mechanical chopper (model 196, Princeton Applied Research, Oak Ridge, TN), and the signal was detected using a digital storage oscilloscope (model 54520A, 500 MHz, Hewlett-Packard, Palo Alto, CA).

Results and Discussion

Powder characteristics will be briefly summarized here but described in full detail in a future publication. Powder XRD data revealed that the solvothermal processes crystallized CaF_2:Er (0.5 mol %) and LaF_3:Nd (0.5 mol %) phases directly from solution. Heat-treating these samples did not reveal any phase heterogeneities. Representative XRD patterns of heat-treated 0.5 mol % Er- and Nd-doped nanocrystalline CaF_2 and LaF_3 are shown in Figure 2a,b. The patterns are well-matched in both relative intensity and position with the reference ICDD XRD data (PDF no. 75-0363 for CaF_2, PDF no. 33-0704 for LaF_2, and PDF no. 32-0483 for LaF_3). Figure 3a,b shows TEM images of the heat-treated nanocrystals containing 0.5 mol % Er in CaF_2 and 0.5 mol % Nd in LaF_3. TEM data show primary particle sizes far less than 100 nm and suggest that these particles may be dispersible at sizes less than 100 nm. CaF_2:Er has substantially larger primary particles on the order of 50 nm while LaF_3:Nd has sizes that are on the order of 10 nm.

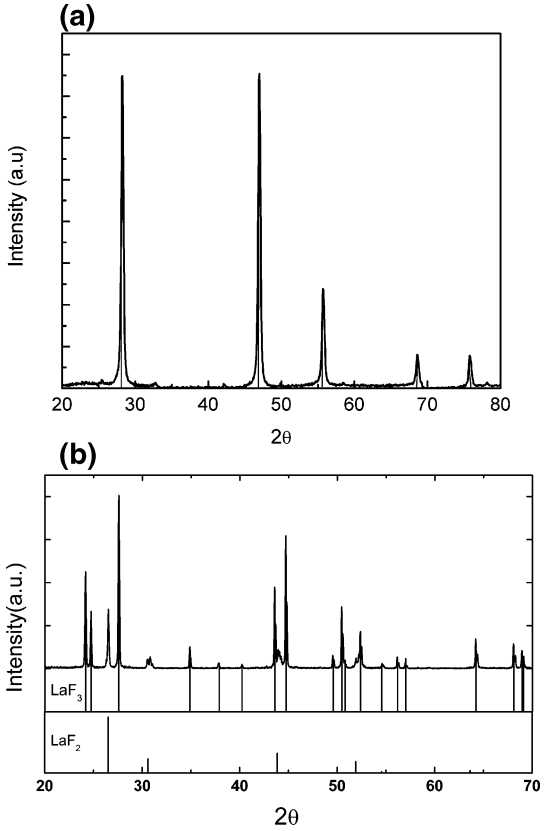

Figure 2. X-ray diffraction patterns of the heat-treated nanocrystals of (a) CaF_2:Er (0.5 mol %) and (b) LaF_3:Nd (0.5 mol %) nanocrystals heat-treated at 800 °C for 2 h. The vertical lines are ICDD diffraction references; PDF no. 75-0363 (CaF_2), PDF no. 33-0704 (LaF_2), and PDF no. 32-0483 (LaF_3).

Figure 4a,b shows the room temperature absorption spectrum of CaF_2:Er (0.5 mol %) and LaF_3:Nd (0.5 mol %) in the UV−vis−NIR region. For optical absorption measurements, the powder was pressed into transparent pellets of 2 mm thickness using a manual pellet press (Carver, Inc., Wabash, IN). The spectra for the nanocrystals show the characteristic absorption bands of Er^{3+} and Nd^{3+} similar to those found for bulk single crystals. The absorption data are used to evaluate the radiative decay time of the infrared emitting bands of Er^{3+} and Nd^{3+} using the well-known Judd−Ofelt procedure.[29,30] The parameters obtained for CaF_2:Er are $\Omega_2 = 7.24 \times 10^{-20}$ cm^2, $\Omega_4 = 0.8 \times 10^{-20}$ cm^2, and $\Omega_6 = 1.24 \times 10^{-20}$ cm^2 and for LaF_3:Nd are $\Omega_2 = 0.93 \times 10^{-20}$ cm^2, $\Omega_4 = 1.84 \times 10^{-20}$ cm^2, and $\Omega_6 = 2.53 \times 10^{-20}$. With these parameters, a radiative decay time of 13.1 ms was computed for the $^4I_{13/2} \rightarrow {}^4I_{15/2}$ transition for Er^{3+}. Similarly for Nd, 846 μs was computed for the $^4F_{3/2} \rightarrow {}^4I_J$ (J = 9/2, 11/2, 13/2, 15/2) transition.

The infrared emission spectra obtained for the two heat-treated samples are shown in Figure 5a,b. CaF_2:Er (0.5 mol %) emission is observed at 1544 nm with an effective spectral bandwidth of 82 nm. With the above computed radiative

(28) Smith, D.; Chen, S.; Kumar, S.; Ballato, J.; Topping, C.; Foulger, S. *Adv. Mater.* **2002**, *14*, 1585.
(29) Judd, B. R. *Phys. Rev. B* **1962**, *127*, 750.
(30) Ofelt, G. S. *J. Chem. Phys.* **1962**, *37*, 511.

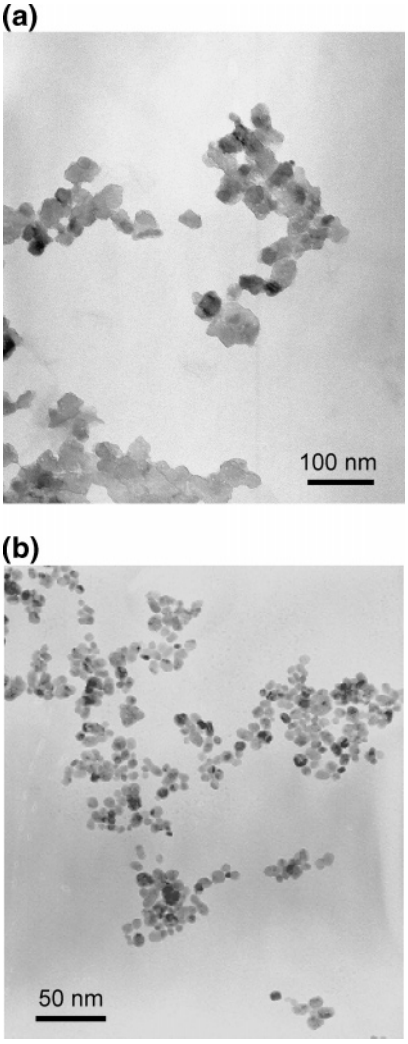

Figure 3. TEM images of nanocrystals of (a) CaF_2:Er (0.5 mol %) and (b) LaF_3:Nd (0.5 mol %).

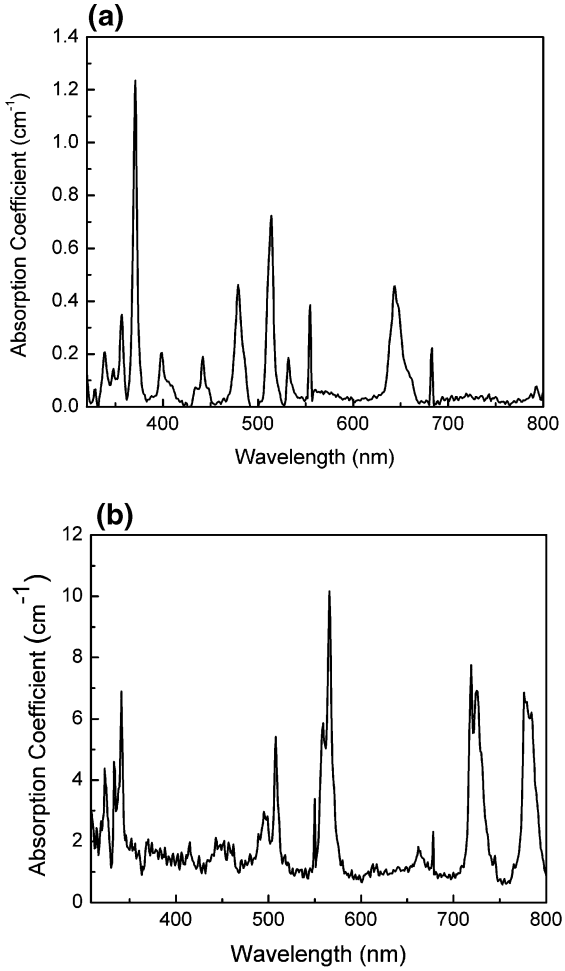

Figure 4. Optical absorption spectrum of (a) CaF_2:Er (0.5 mol %) and (b) LaF_3:Nd (0.5 mol %).

decay time, a stimulated emission cross section of 0.35×10^{-20} cm^2 is obtained for 1544 nm emission, which is comparable to that of single-crystal CaF_2:Er (3.48×10^{-3} mol % Er).[31] For LaF_3:Nd (0.5 mol %), the excitation of the $^4F_{3/2}$ band at 800 nm yields four emission bands at 920, 1070, 1320, and 1808 nm with the transitions shown in the inset of Figure 5b. The fluorescence branching ratios of these bands are 6.6% (920 nm), 51.4% (1070 nm), 20.4% (1320 nm), and 19.0% (1808 nm), with corresponding stimulated emission cross sections of 0.09×10^{-20} cm^2, 0.34×10^{-20} cm^2, 1.35×10^{-20} cm^2, and 0.25×10^{-20}cm^2, respectively.

In order to measure the quantum efficiency of the observed emission bands, the excitation laser pulse was modulated and the luminescence signal was collected and averaged using an oscilloscope. The decay curves obtained are shown in Figure 6a,b for the 1544 nm emission of CaF_2:Er (0.5 mol %) and 1070 nm emission of LaF_3:Nd (0.5 mol %). The lifetimes obtained from nonlinear curve fitting are 7.0 ms for Er^{3+} (0.5 mol %) and 800 μs for Nd^{3+} (0.5 mol %). These lifetimes, together with the calculated radiative decay times, yield a radiative quantum efficiency of 51% for CaF_2:Er (0.5 mol %) and 95% for LaF_3:Nd (0.5 mol %) at 1070 nm. The obtained lifetime values are in reasonable agreement with the earlier reported values of CaF_2:Er (8.5 ms at 3.5×10^{-3} mol % Er) and LaF_3:Nd (0.5 mol %) single crystals.[31,32] Fan and Kokta[33] reported the upper state lifetime of Nd^{3+} in LaF_3 as 735 μs for 0.5 mol %, 675 μs for 1 mol %, and 445 μs for 3 mol % doping at room temperature. Recently Stouwdam and Van Veggel[25] reported a fluorescence decay time of 240 μs for LaF_3:Nd (5 mol %) nanocrystals.

Spectral analysis of samples ranging in rare-earth concentration from 0.5 to 16.7 mol % shows that 0.5 mol % dopant concentrations exhibit the highest quantum efficiency, which are 51 and 95% for CaF_2:Er and LaF_3:Nd (Figure 7). Quantum efficiency reduces significantly at concentrations above this value because of concentration quenching. Concentration quenching results from nonradiative energy transfer interactions between nearby rare-earth ions. For example, the probability of an energy transfer via a dipole−dipole interaction mechanism varies as the inverse of the sixth power of the rare-earth interionic separation.[5]

Other sources of nonradiative losses are the surface hydroxyls (bulk and surface species) and defects. Hydroxyls play a major role in the fluorescence quenching of infrared

(31) Kumar, G. A.; Riman, R. E.; Chae, S. C.; Jang, Y. N.; Bae, I. K.; Moon, H. S. *J. Appl. Phys.* **2004**, *95*, 3243.

(32) Kaminski, A. A. *Laser Crystals-Their Physics and Properties*; Springer: Berlin, 1989.

(33) Fan, T. Y.; Kokta, M. R. *IEEE J. Quantum Electron.* **1989**, *25*, 1845.

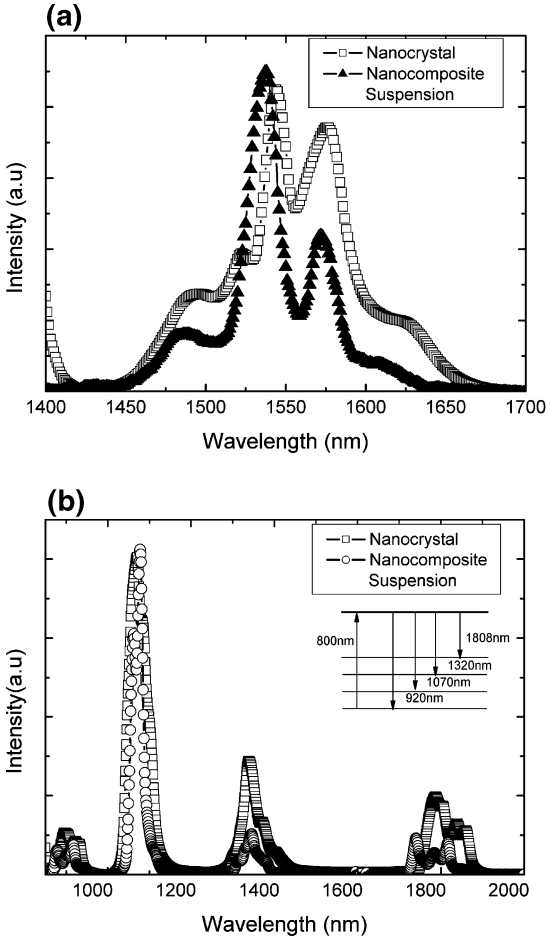

Figure 5. Infrared emission spectra of (a) Er^{3+} (0.5 mol %) in CaF_2 nanocrystal and its suspension in PFCB-6F-in-THF solution (excitation wavelength 980 nm) and (b) Nd^{3+} (0.5 mol %) in LaF_3 nanocrystal and its suspension in PFCB-6F-in-THF solution (excitation 800 nm; transition scheme shown in inset.

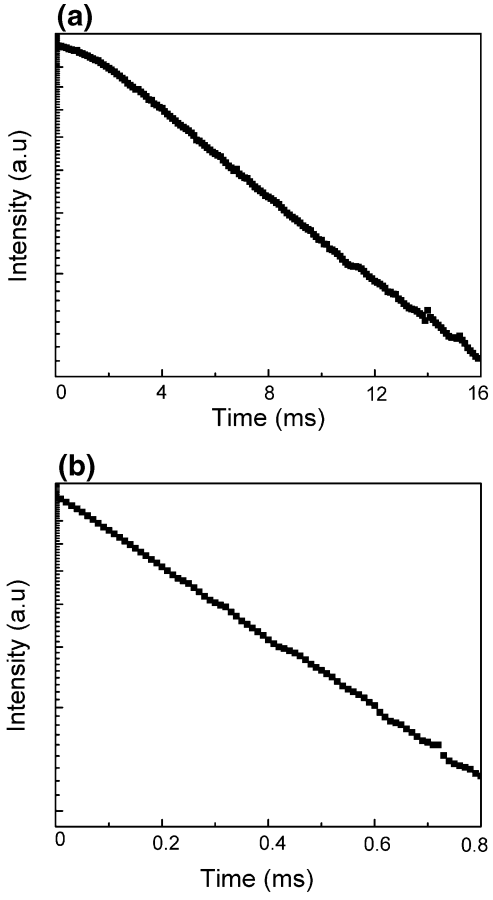

Figure 6. Fluorescence decay of the (a) 1544 nm emission of CaF_2:Er (0.5 mol %) and (b) 1070 nm emission for in LaF_3:Nd (0.5 mol %).

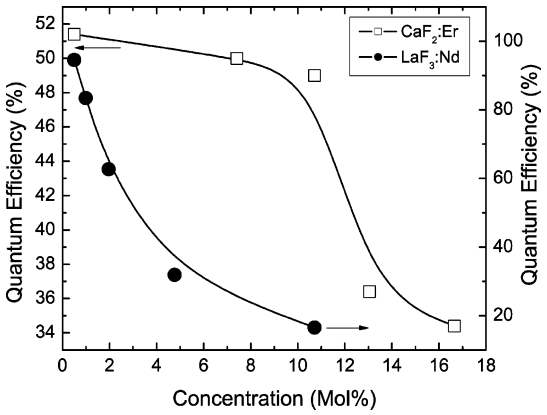

Figure 7. Fluorescence quenching in CaF_2:Er and LaF_3:Nd as a function of the rare-earth concentration.

emission in rare-earth-doped materials.[34] The first-order vibrational overtone of O−H (2900 nm (3400 cm^{-1})) is strongly resonant with the $^4I_{13/2} \rightarrow {}^4I_{15/2}$ transition (1550 nm (6500 cm^{-1})) of Er^{3+}. Similarly the second-order vibrational overtone of O−H is almost in resonance with the $^4F_{3/2} \rightarrow {}^4I_{13/2}$ transition (1345 nm (7434 cm^{-1})), and hence the presence of OH primarily influences the 1340 nm (7462 cm^{-1}) emission. Infrared spectra for the rare-earth-doped halide powders show these OH absorptions and, hence, the presence of hydroxyl species. Heat treatment of these powders at 800 °C reduced the OH absorptions, which increased the emission intensity substantially. However, the increment was more pronounced in the case of LaF_3:Nd nanoparticles. This may be attributed to reducing rare-earth ion clustering in LaF_3 nanoparticles relative to the CaF_2 host.

Defects in the nanocrystals are also an important factor. First, the high surface to volume ratio for nanocrystals renders the surface species as a major fraction of the population. Surfaces are well-known to comprise all types of defects such as dangling bonds, adsorption of impurity species, and regions of disorder. In addition, it is particularly relevant to also point out that rare-earth-doped nanocrystals may also exhibit surface excesses of rare-earth species. This would cause the interionic spacing to be small and hence quench desired transitions. Another possibility is the adsorption of high phonon energy species such as solvothermal solvents such as 1,4-butanediol or ethylene glycol.

Both LaF_3:Nd and CaF_2:Er polymer PFCB-6F nanocomposite systems in solution and polymer media show excellent transparency (Figure 8a,b). The excellent transmissions (low losses) for these nanocomposites are attributed to both the small dispersed particle size and/or low index mismatch between the nanocrystal and the polymer matrix. The Rayleigh equation illustrates this, where spherical particles have sizes assumed to be smaller than the wavelength of

(34) Banerjee, S.; Huebner, L.; Romanelli, M. D.; Kumar, G. A.; Riman, R. E.; Emge, T. J.; Brennan, J. G. *J. Am. Chem. Soc.* **2005**, *127*, 15900.

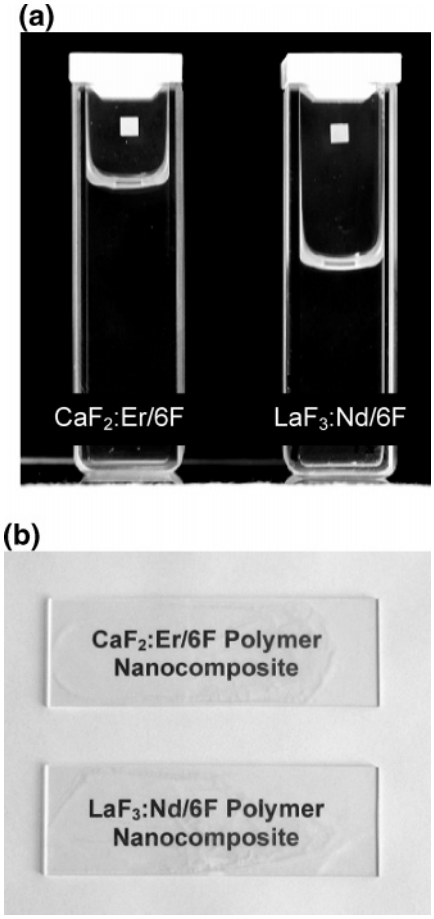

Figure 8. Photographs of transparent (a) CaF_2:Er and LaF_3:Nd suspended in PFCB-6F-in-toluene solutions and (b) CaF_2:Er/6F and LaF_3:Nd/6F polymer nanocomposites.

scattered light and each particle functions as an independent scatterer.[35] Using the Rayleigh equation, the scattering loss per unit length as a function of the particle size was computed for CaF_2:Er and LaF_3:Nd in PFCB-6F. A dilute concentration of 0.2 vol % was assumed for illustrative purposes since higher concentrations such as those used in our composites (~0.4 vol %) might be susceptible to multiple scattering, thereby invalidating the use of the Rayleigh equation. Figure 9 shows that the scattering loss rapidly increases with increasing particle size to the third power and linearly with the square of the refractive index mismatch between the nanoparticles and the surrounding host. Assuming all the optical loss is attributed to independent scattering, a CaF_2:Er/PFCB-6F nanocomposite with 20 nm nanocrystals has a loss of 0.025 dB/cm. In contrast, the scattering loss increases to 35 dB/cm for a LaF_3:Nd/PFCB-6F nanocomposite. The large difference in scattering loss is attributed the larger refractive index mismatch for LaF_3:Nd/PFCB-6F ($\Delta n \sim 0.2$) than for CaF_2:Er/PFCB-6F ($\Delta n \sim 0.034$). For a composite

(35) Rayleigh, J. W. S. *Philos. Mag.* **1881**, *12*, 81.

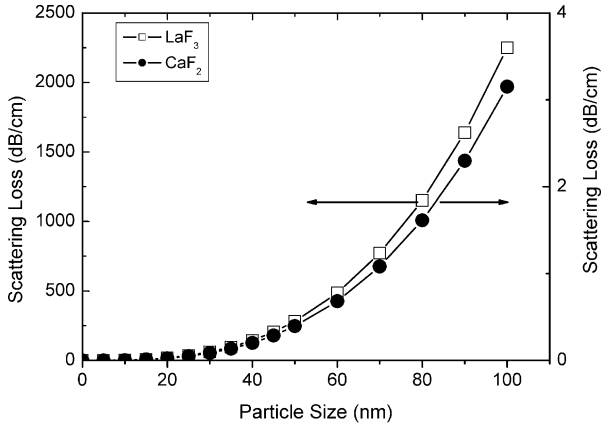

Figure 9. Scattering loss per unit length as a function of particle size for CaF_2:Er/6F (wavelength is 1060 nm) and LaF_3:Nd/6F 0.2 vol % nanocrystals (wavelength is 1540 nm).

based on 20 nm particles, the percent transmissions of CaF_2:Er/6F are 99% and 80% for LaF_3:Nd. When a loss of 1 dB/cm is assumed to be a critical value to remain below, nanocomposites based on 0.2 vol % LaF_3:Nd require 6.8 nm particle sizes while those based on CaF_2:Er require 70 nm. Clearly, nanocomposites based on calcium fluoride can tolerate larger particle sizes than lanthanum fluoride. This work also shows the importance of dispersing all particle sizes at length scales below 100 nm when the index differences are 0.2 or less. Thus, it likely that both samples had dispersion particle sizes less than 100 nm, if not substantially less than 100 nm. Future work will focus on obtaining quantitative data to demonstrate this more conclusively using more quantitative methods.

Conclusions

Highly emissive halide nanopowders (LaF_3:Nd and CaF_2:Er) were prepared by solvothermal methods. Dopant concentrations of 0.5 mol % rare-earth species exhibit quantum efficiencies as high as 95% for LaF_3:Nd and 51% for CaF_2:Er, while higher concentrations exhibit lower quantum efficiencies. Light scattering computations, visual suspension and composite transparency, and TEM data suggest that composites were prepared with dispersed particle sizes less than 100 nm. In order to maintain low transmission loss, nanocomposites based on LaF_3:Nd require far smaller particle sizes than CaF_2 because of their larger index difference compared to that of the PFCB-6F matrix.

Acknowledgment. The authors would like to acknowledge the support of the Office of Naval Research, The New Jersey State Commission on Science and Technology, and USR Optonix, Inc., Sunstones, Inc., and the U.S. Army through the South Carolina Research Authority (sub-recipient Agreement No. 2001-509, task order 0007, Active Coatings Technology program). In addition, we wish to thank Tetramer Technologies, LLC, for generously supplying PFCB-6F polymer.

CM051567N